



Mechanistic investigation of a D to N mutation in DAHP synthase that dictates carbon flux into the shikimate pathway in yeast

Huayi Liu ^{1,2}, Qingjie Xiao³, Xinxin Wu¹, He Ma¹, Jian Li¹, Xufan Guo¹, Zhenyu Liu¹, Yan Zhang⁴ & Yunzi Luo ^{1,2}✉

3-deoxy-D-arabino-heptulosonate-7-phosphate synthase (DAHPS) is a key enzyme in the shikimate pathway for the biosynthesis of aromatic compounds. L-Phe and L-Tyr bind to the two main DAHPS isoforms and inhibit their enzyme activities, respectively. Synthetic biologists aim to relieve such inhibitions in order to improve the productivity of aromatic compounds. In this work, we reported a point mutant of yeast DHAPS, Aro3^{D154N}, which retains the wild type enzyme activity but converts it highly inert to the inhibition by L-Phe. The Aro3 crystal structure along with the molecular dynamics simulations analysis suggests that the D154N mutation distant from the inhibitor binding cavity may reduce the binding affinity of L-Phe. Growth assays demonstrated that substitution of the conserved D154 with asparagine suffices to relieve the inhibition of L-Phe on Aro3, L-Tyr on Aro4, and the inhibitions on their corresponding homologues from diverse yeasts. The importance of our discovery is highlighted by the observation of 29.1% and 43.6% increase of yield for the production of tyrosol and salidroside respectively upon substituting *ARO3* with *ARO3^{D154N}*. We anticipate that this allele would be used broadly to increase the yield of various aromatic products in metabolically diverse microorganisms.

¹Frontiers Science Center of Synthetic Biology and Key Laboratory of Systems Bioengineering (Ministry of Education), School of Chemical Engineering and Technology, Tianjin University, Tianjin 300072, China. ²Georgia Tech Shenzhen Institute, Tianjin University, Tangxing Road 133, Nanshan District, Shenzhen 518071, China. ³National Facility for Protein Science in Shanghai, Shanghai Advanced Research Institute (Zhangjiang Laboratory), Chinese Academy of Sciences, Shanghai 201210, China. ⁴Tianjin Key Laboratory for Modern Drug Delivery & High-Efficiency, Collaborative Innovation Center of Chemical Science and Engineering, School of Pharmaceutical Science and Technology, Tianjin University, Tianjin 300072, China. ✉email: yunzi.luo@tju.edu.cn

Plants and microbes use the shikimate pathway as the biosynthetic route to produce aromatic amino acids (AAAs), while animals rely on acquisition of essential AAAs from their foods. Therefore, the prevalence of the shikimate pathway rivals that of nitrogen fixation and photosynthesis. More importantly, the shikimate pathway is employed by plants and microbes as early steps where they branch out to synthesize a great variety of natural products with aromatic ring components, with many of them being highly valuable and widely used in foods, nutraceuticals, cosmetics, and pharmaceuticals such as phenylethanoids, resveratrol, flavonoids and alkaloids^{1–4}.

In the seven-step shikimate pathway, the first committed step involves an aldol condensation of PEP and E4P to form DAHP, catalyzed by DAHPS, which can be classified into Type I and Type II enzymes based on their sequence relationships⁵. Type I DHAPS is further divided into Type Ia and Ib. Commonly used model organisms and industrial fermentation strains such as *Escherichia coli* (*E. coli*) and *Saccharomyces cerevisiae* (*S. cerevisiae*) contain Type Ia DHAPS, which is allosterically regulated and feedback inhibited by downstream AAAs¹. For example, the two isomeric Type Ia DAHPSs, Aro3/Aro4 of *S. cerevisiae* and AroG/AroF of *E. coli*, are feedback inhibited by L-phenylalanine (L-Phe) and L-tyrosine (L-Tyr), respectively (Fig. 1A)^{6–8}.

Overexpression of Aro4^{K229L}, a mutant resistant to the feedback inhibition of L-Tyr, has been commonly used as a strategy to successfully unlock the carbon flux into the shikimate pathway, resulting in higher yields of aromatic products in engineered *S. cerevisiae* strains^{1,7,9}. However, the beneficial effects of the analogous Aro3 mutant, ARO3^{K222L} have been controversial. Significantly increased production of protocatechuic acid has been observed¹⁰, while no notable increase of the yields of tyrosol, salidroside, 2-phenylethanol, and chlorogenic acid have been reported by others and us^{11–13}. The detailed mechanism that how Aro4^{K229L} could relieve the feedback inhibition of L-Tyr remains unclear. Nevertheless, the discrepancy indicates that Aro3 and Aro4 differ in the responses to the inhibitors of their own and that Aro3^{K222L} may not fully relieve the feedback inhibition of L-Phe in *S. cerevisiae*.

In search for an Aro3 mutant that is insensitive to the feedback inhibition of L-Phe to overcome the bottleneck for the flux into the shikimate pathway, we noticed that a point mutation D146N located apart from the inhibitor binding pocket of AroG has been commonly used to relieve the feedback inhibition of L-Phe to

overproduce aromatic products in *E. coli*^{1,8,14}. Inspired by this, Aro3^{D154N} that is an equivalent to the D146N mutant of the *E. coli* isozyme AroG was designed. Structural, computational, and biochemical characterization of this mutant unravels its mechanism in efficiently eliminating the feedback inhibition of L-Phe on Aro3 in yeast. This mechanism also explains our observation that an analogous mutation to the conserved Asp in Aro4 or other homologs from various yeast strains works equally well in alleviating the feedback inhibition either from L-Tyr or L-Phe, including non-conventional industrial yeasts. The generality expands the enzyme toolbox for production of diverse aromatic compounds in a great variety of microbial cell factories, including model hosts and non-conventional hosts. To demonstrate its potential, we introduced this allele to engineered *S. cerevisiae* strains that overproduce tyrosol and salidroside respectively, resulting in further significantly increased yields.

Results

Relieve of the feedback inhibition on Aro3 by overexpression of Aro3^{D154N} in *S. cerevisiae*. Aro3^{K222L} and Aro3^{D154N} were constructed and used to substitute the wild-type Aro3 of *S. cerevisiae* in situ, respectively. The promoter of ARO3 was exchanged to the constitutive *TEF1* promoter to remove the transcription regulation¹⁵. To assess Aro3 mutants without interference by Aro4, Aro3 mutants were overexpressed in *aro4Δ* background strain A3_1 (Supplementary Table 1). The extracellular titers of aromatic fusel alcohols, tyrosol, 2-phenylethanol, and tryptophol, belonging to the L-Tyr, L-Phe, and L-Trp branch products respectively, were measured as indicatives of the carbon flux of AAAs biosynthesis pathway⁷ (Fig. 1). Aro3^{K222L} overexpressing did not increase the yield of any of the three compounds (Fig. 1B). By contrast, Aro3^{D154N} significantly increased the titers of aromatic products (over 300% increase for tyrosol and 50% for 2-PE, no increase of tryptophol observed because of the *trp1Δ* mutation in the WT strains) (Fig. 1B). Furthermore, the titers of AAA derivatives in the A3_1 strain with a D154N mutation in the endogenous ARO3 were comparable to those in the strain carrying the wild-type ARO3 and an additional copy of ARO3^{D154N} integrated at a different locus of the genome, suggesting that this is a dominant mutant in abolishing the feedback inhibition (Fig. 1B).

Next, we decided to test if the increased yield of aromatic fusel alcohols is a result of ARO3^{D154N} relieved from the feedback

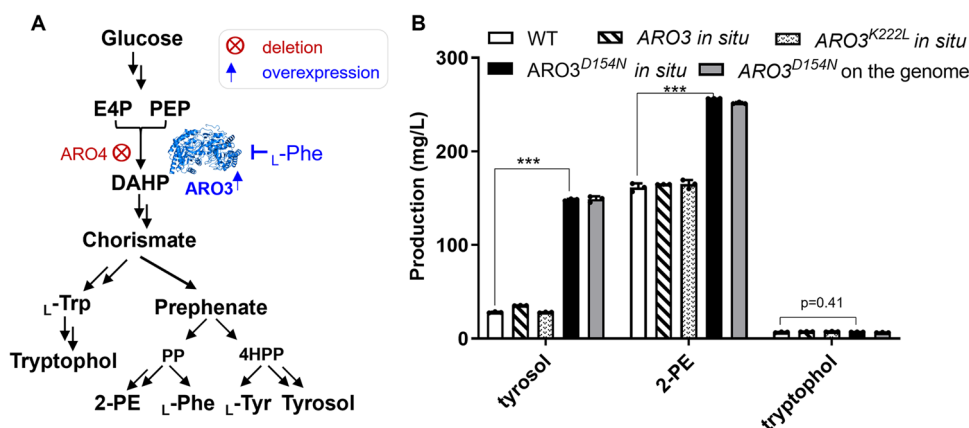


Fig. 1 The impact of the overexpression of ARO3 mutants on the production of aromatic amino acid derivatives. **A** The biosynthetic pathways of tryptophol, tyrosol, and 2-phenylethanol. The double arrows represent multiple enzymatic steps. Metabolite abbreviations: PEP, phosphoenol pyruvate; E4P, erythrose 4-phosphate; DAHP, 3-deoxy-D-arabino-heptulosonate-7-phosphate; L-Trp, L-tryptophan; L-Tyr, L-tyrosine; L-Phe, L-phenylalanine; 4-HPP: 4-hydroxyphenylpyruvate; PP: phenylpyruvate; 2-PE, 2-phenylethanol. **B** The extracellular concentrations of tryptophol, tyrosol, and 2-PE through the overexpression of ARO3, ARO3^{K222L}, and ARO3^{D154N} in situ or through the addition copy of ARO3^{D154N} on the genome. Error bars represent the standard deviation (\pm SD) of three biological repeats. Source data are available in Supplementary Data 4. *** $p < 0.001$.

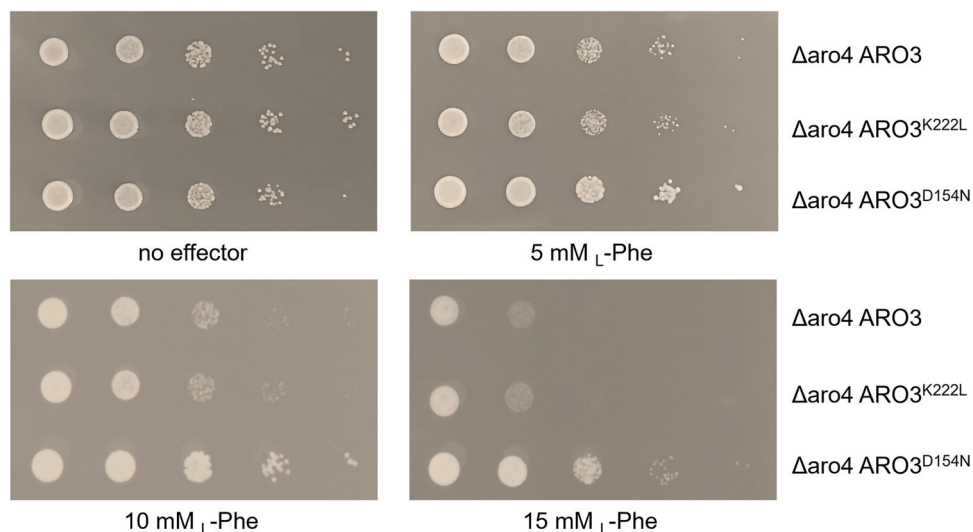


Fig. 2 Growth of different yeast strains carrying various Aro3 mutants. To compare the effects of different Aro3 mutants, the yeast strains were cultivated in MV liquid medium, harvested at 36 h, diluted at $OD_{600} = 1.0$, and serially 10-fold diluted to spot onto the MV solid medium in the presence or absence of 5 mM, 10 mM, and 15 mM L -Phe. Plates were incubated at 30 °C for 60 h.

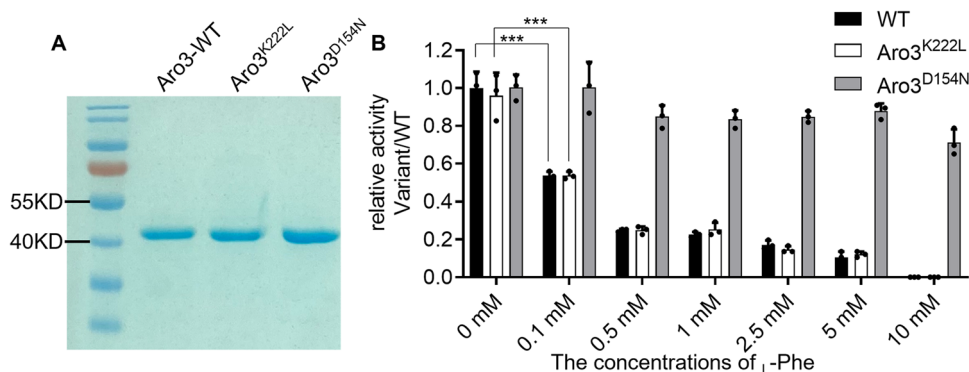


Fig. 3 Activities of purified Aro3 enzymes in the presence and absence of L-phenylalanine. **A** The SDS-PAGE evaluation of recombinant proteins of Aro3, Aro3^{K222L}, and Aro3^{D154N}. See Supplementary Figure 2 for the uncropped SDS-PAGE image. **B** Relative activities of recombinant Aro3 variants in the presence or absence of L -Phe. The activities were measured in the presence of 0 to 10 mM of the L -Phe. Activity of the wild-type Aro3 without effector was set to 1.0. Error bars represent the standard deviation of three biological repeats. Source data are available in Supplementary Data 4. *** $p < 0.001$.

inhibition by L -Phe. Plate assays were performed with added aromatic amino acids to the growth media. The *TRP1* gene was repaired in A3_1 strain to resume L -Trp synthesis, generating A3_4 strain (CEN.PK2-1C Δ aro4 *TRP1* P_{TEF1}-ARO3). Growth of the parental A3_4 strain was inhibited by L -Phe, but not L -Tyr nor L -Trp (Fig. 2, Supplementary Figure 1). Such unique L -Phe sensitivity persists through the overexpression of the ARO3^{K222L} allele but could be relieved by introducing the ARO3^{D154N} allele (Fig. 2 and Supplementary Figure 1).

Enzyme activity of Aro3^{D154N}. For in vitro biochemical and biophysical characterization of the enzymes, we recombinantly produced and purified Aro3 and its two variants, Aro3^{K222L} and Aro3^{D154N} (Fig. 3). The three enzymes exhibited comparable activity in the absence of L -Phe (Fig. 3B). Low concentration of L -Phe (0.1 mM) inhibited the enzyme activity of wild-type Aro3 and Aro3^{K222L} by half, but did not affect Aro3^{D154N} activity (Fig. 3B). High concentration of L -Phe (10 mM) completely abolished the activity of wild-type Aro3 and Aro3^{K222L}, while Aro3^{D154N} retained the majority of its enzyme activity (71.2%) (Fig. 3B). Taken together, Aro3 activity is allosterically inhibited by L -Phe and we demonstrated that the inhibition could be rescued by a D154N single point mutation.

Molecular basis of relieved allosteric inhibition. To further investigate the mechanism of the D154N mutation in relieving the inhibition by L -Phe, we determined the crystal structure of Aro3 at 3.3 Å (Table 1). The Aro3 crystals contain one dimer per asymmetric unit with each monomer exhibiting a canonical (β/α)₈ TIM-barrel fold common to other Type Ia DAHPS enzymes (Supplementary Figure 3)^{6,14,16–20}. Next, we used the AutoDockTools-1.5.6 program to model the complex structures. Two available isozyme-ligand complex structures, AroG from *E. coli* (PDB code: 1KFL) and NmDAHPS from *Neisseria meningitidis* (PDB code: 4UC5) are used for comparison with our docking model. The positioning of the Phe and its interacting residues of the two complex crystal structures and our docking model can be overlaid nicely (Supplementary Figure 4). Then the docking model was applied to perform unconstrained molecular dynamics (MD) simulations (1000 ns). After the RMSD of the C α atoms reached equilibrium, the last 650 ns of each trajectory was subjected to further analysis (Supplementary Figure 5). During the simulations, L -Phe was harbored in a cavity formed by helices α 3 and α 4, β -sheets of β 6a/ β 6b and their adjacent loops, and the N-terminus of the second subunit of the dimer. Strikingly, the distance between the carboxyl oxygen (OE1) of Q159 and the nitrogen (N) of L -Phe was centered

Table 1 Data collection and refinement statistics (molecular replacement).

	Aro3
<i>Data collection</i>	
Space group	P 2 21 21
Cell dimensions	
<i>a</i> , <i>b</i> , <i>c</i> (Å)	73.68, 95.561, 105.785
α , β , γ (°)	90, 90, 90
Resolution (Å)	105.79–3.3 (3.56–3.3) ^a
<i>R</i> _{sym} or <i>R</i> _{merge}	0.115 (1.503)
<i>I</i> / σ <i>I</i>	9.6 (1.3)
Completeness (%)	96.6 (95.9)
Redundancy	7.0 (7.3)
<i>Refinement</i>	
Resolution (Å)	34.37–3.3 (3.418–3.3)
No. reflections	11,322 (1145)
<i>R</i> _{work} / <i>R</i> _{free}	0.252/0.295
No. atoms	
Protein	5760
Ligand/ion	0
Water	0
<i>B</i> -factors	
Protein	176.3
Ligand/ion	0
Water	0
R.m.s. deviations	
Bond lengths (Å)	0.013
Bond angles (°)	1.76

^aNumber of xtals for each structure should be noted in footnote. Values in parentheses are for highest-resolution shell.

around 2.8 Å in the wild-type complex, while a much longer distance (centered around 5.3 Å and 5.8 Å) was found in the Aro3^{D154N} mutant complex (Fig. 4A). The distance between the nitrogen of the ϵ -amino group (NZ) of K222 and the nitrogen of L -Phe was also increased from 4.3 Å in the wild-type complex to 4.7 Å in the Aro3^{D154N} mutant complex (Fig. 4B). Taken together, the hydrogen bonding between L -Phe with the two key residues (Q159 and K222) of Aro3 were weakened by introducing the D154N mutation. We computed the free energy landscape (FEL) of the wild-type and Aro3^{D154N} mutant complexes based on the radius of gyration (Rg) for the dimer of Aro3 and the RMSD of Ca atoms. In the extracted typical conformations of local energy minima based on FEL analysis, longer distances between the two key residues (K222 and Q159) of Aro3^{D154N} and the nitrogen of L -Phe were found in the mutant Aro3 complex (Fig. 4E, F, 4.7 Å/5.7 Å) compared to the corresponding distances in the wild-type complex (Fig. 4C, D, 4.2 Å/2.8 Å). Structural analyses suggested that the binding affinity for L -Phe was reduced by the single D154N point mutation.

We next employed isothermal titration calorimetry (ITC) to quantitatively characterize the interactions between Aro3 and Aro3^{D154N} with L -Phe. The two recombinant Aro3 forms showed enthalpy-driven binding of L -Phe with physiologically relevant *K*_d (Fig. 5). Among them, the wild-type enzyme demonstrated high binding affinity for L -Phe with a *K*_d of 31.4 μ M. The mutant Aro3^{D154N} exhibited weaker interactions and higher *K*_d value, 10-fold of the wild-type *K*_d. The ITC measurements are consistent with the observation that D154N reduced the binding affinity for L -Phe in MD stimulations.

The D to N mutation in other type Ia DAHPS enzymes. Sequence alignments of DAHPS enzymes revealed high conservativity of the Asp residue corresponding to the D154 of yeast Aro3 (Supplementary Figure 6). Considering that all type Ia

DAHPS enzymes with known structures share highly similar overall folding and domain architectures⁵, we decided to test the effects of substituting this residue with Asn in other enzymes of this family. We started the investigation of Ia DAHPS from commonly used model organisms known to be inhibited by L -Tyr instead of L -Phe, including Aro4 from *S. cerevisiae* and AroF from *E. coli*. We constructed Aro4^{D161N} and AroF^{D147N} and examined them in the established plate assays. Overexpression of both mutants recovered growth inhibited by L -Tyr (Supplementary Figure 7). Strikingly, Aro4^{D161N} was found as effective as Aro4^{K229L} (Supplementary Figure 7) that is widely used to unlock carbon flux into the AAAs biosynthetic pathway in yeast¹.

We next expanded our studies with focuses on type Ia DAHPS enzymes from various organisms that are not conventionally used in industry, including Q6CCS4 and Q6CDZ3 from *Yarrowia lipolytica*, C4QXT0 and C4R611 from *Komagataella phaffii* GS115 (*Pichia pastoris*), W0T5I6 and W0TBD2 from *Kluyveromyces marxianus* strain DMKU3-1042 (*Candida kefyr*), W1QFS3 and W1QII3 from *Ogataea parapolymorpha* strain ATCC 26012 (*Hansenula polymorpha*). Some unique properties of these microbial organisms were recently appreciated and they started being used as microbial cell factories^{21–24}. However, lack of knowledge about their type Ia DAHPS enzymes and methods to bypass the allosteric inhibition impedes boosting carbon flux into the shikimate pathway for the high yield production of aromatic compounds. According to previous studies, among all our tested enzymes, Q6CDZ3, C4R611, W0TBD2, and W1QII3 contain a serine residue corresponding to the Ser219 of yeast Aro3 and are likely sensitive to L -Phe, while a glycine residue at the same position in Q6CCS4, C4QXT0, W0T5I6, and W1QFS3 may confer their sensitivity to L -Tyr inhibition^{6,19,20}. Our plate assays with engineered yeast strains carrying the WT forms of these DAHPS enzymes confirmed such inhibitor specificities (Supplementary Figure 8). We next tested the D to N mutant forms of these enzymes, despite the differences of the inhibitors and the origins of the enzymes, a D to N single amino acid residue substitution demonstrated strong efficacy in relieving the growth inhibition by the enzyme inhibitor (Fig. 6).

Metabolomic studies of the ARO3^{D154N} overexpressing strain.

Next, we performed metabolomic analyses on the ARO3^{D154N} overexpressing strain (strain A3_3) with the origin CEN.PK2-1C strain and wild-type ARO3 overexpressing strain as controls. We examined both intracellular and extracellular concentrations of AAAs derivatives including anthranilic acid, phenylpyruvic acid, L -tyrosine, and tyrosol. It was found that all of them increased significantly in the ARO3^{D154N} overexpressing strain but not in the wild-type ARO3 overexpressing strain in comparison with the origin CEN.PK2-1C strain levels. By contrast, the concentrations of metabolites that branch out from PEP decreased in the ARO3^{D154N} overexpressing strain. These include intracellular 2-isopropylmalate, acetic acid, L -aspartic acid, GABA (γ -aminobutyric acid), L -proline, L -ornithine, and L -arginine, and extracellular glutamine (Fig. 7 and Supplementary Figures 9–10). The observation that metabolites of remarkably lowered concentrations are downstream products of the pyruvate metabolism in *S. cerevisiae* (Fig. 7), indicates that overexpression of ARO3^{D154N} shuttles carbon fluxes from pyruvate metabolism to the synthesis of AAAs.

Effects of ARO3^{D154N} overexpression in tyrosol and salidroside overproducing engineered strains. Tyrosol and salidroside are widely used as ingredients of functional foods, cosmetics, and medicines owing to their anti-oxidative and many other properties beneficial to human health^{25,26}. Historically, our laboratory

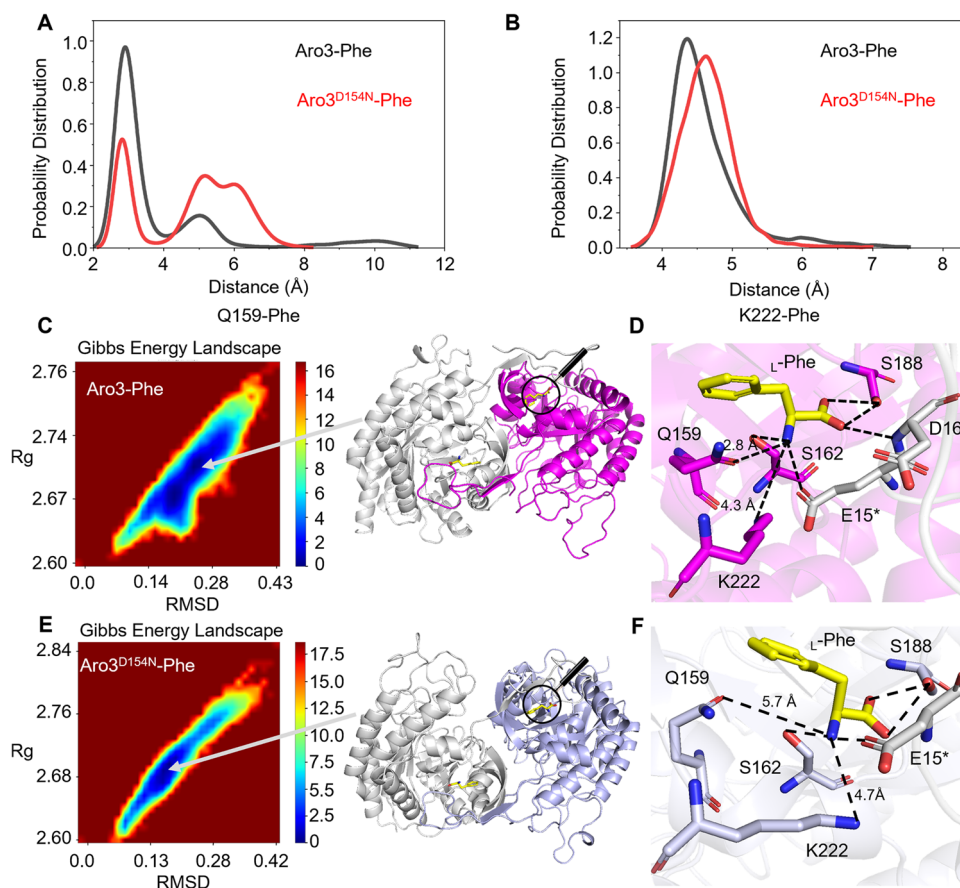


Fig. 4 The molecular dynamics (MD) simulations analysis of Aro3-Phe and Aro3^{D154N}-Phe. **A** Distribution of the distances between Q159 and _L-Phe. **B** Distribution of the distances between K222 and _L-Phe. Frequency distribution of the distances for the wild-type Aro3 (black) and Aro3^{D154N} (red). The distances are calculated using the carboxyl oxygen (OE1) of Q159, the nitrogen of the ϵ -amino group (NE) of K222 and the nitrogen (N) of _L-Phe. The last 150 ns of simulation of each MD runs was used for analysis. **C, E** The free energy landscape (FEL) diagram as a function of RMSD of C α atoms and Rg for the dimer of Aro3 as the two reaction coordinates of Aro3-Phe (**C**) and Aro3^{D154N}-Phe (**E**). The typical snapshots from corresponding minimum energy wells were extracted. **D, F** Zoomed-in view of the distances between Q159/K222 and _L-Phe of Aro3-Phe (**D**) and Aro3^{D154N}-Phe (**F**) in the corresponding extracted conformation. The side chains of the _L-Phe binding residues are shown as sticks and the residues marked as asterisk (*) belong to different subunits of Aro3 dimer. The _L-Phe was shown as yellow sticks. Oxygen and nitrogen are shown in red and blue respectively. Black dotted lines indicate hydrogen bonds.

constructed a yeast strain, namely TY4 with a high yield of tyrosol²⁷ (Fig. 8A). We used TY4 as a chassis to overproduce salidoside based on our discovery that glycosylation of tyrosol to form salidoside is efficiently catalyzed by a glycosyltransferase from *Rhodiola rosea*, the RrU8GT33¹¹ (Fig. 8A). Integration of the overexpressing ARO3^{D154N} cassette into TY4 produces TY5, which results in a 29% increase of tyrosol titer, reaching record-high 1.3 g/L. By comparison, overexpression of the wild-type ARO3 or ARO3^{K222L} did not show statistically significant effects (Fig. 8B). TY4 and TY5 were engineered to overexpress RrU8GT33 as previously reported¹¹, and compared with each other for salidoside production. Overexpression of ARO3^{D154N} was noticed to increase salidoside production by 44%, reaching 2.4 g/L, which is also the highest ever reported in flask fermentation (Fig. 8C). The products of tyrosol and salidoside was confirmed by LC-MS/MS and by comparing with standard compounds (Supplementary Figures 11–12).

Discussion

The feedback inhibition-resistant mutant Aro4^{K229L} has been widely used in yeast engineered for aromatic compound overproduction¹, whereas report of Aro3 allele for similar purposes was rare. Christine Brückner et al. showed that the

overexpression of an analogous Aro3 mutant, Aro3^{K222L} increased the yield of protocatechuic acid¹⁰. It is intriguing that studies by others and the present work failed in observing any positive effect of Aro3^{K222L} mutant^{11–13}. The discrepancy could have been due to usage of different yeast genetic backgrounds. We chose the *aro4* deleting strain in order to avoid interference by its specific inhibitor _L-Tyr, while the Brückner group used a strain deletion of AroE that encodes the E-domain of Aro1 with dehydrogenase activity. Deletion of AroE hinders the carbon fluxes towards AAA biosynthetic pathway, thus decreases the intracellular concentration of _L-Phe¹⁰. Perturbation by AroE deletion makes interpretation of the data difficult, given that _L-Phe inhibition on Aro3 is dose-dependent. It was also noted that the Brückner group codon-optimized ARO3^{K222L}, but not the control ARO3 sequence as stated by themselves, which may have resulted in different expression levels of the two enzyme versions accounting for different yields of protocatechuic acid. Nevertheless, no positive effects of ARO3^{K222L} were observed in any of our in vivo systems, where genomic sequences were used in constructing the overexpression of both ARO3 and its mutants to avoid potential variables of protein levels. Furthermore, our results of the in vitro enzyme activity assays using recombinant proteins allowing accurate quantitation should have been more conclusive.

The crystal structure of Aro3 and its modeled complex with Phe reported in this study allow comparison with the yeast Aro4 Tyr complex structure (PDB: 1OF6), which helps to interpret why *ARO4*^{K229L} relieves feedback inhibition and *ARO3*^{K222L} doesn't^{6,18}. Tyr differs from Phe by its 4-OH group. Despite high similarity of inhibitor-enzyme interactions in both complexes, hydrogen bonding between the 4-OH group of Tyr and the

backbone carbonyl group of T162 in Aro4 is absent in the Phe-Aro3 complex (Supplementary Figure 13). This interaction acts in concert with the K229L mutation to position Tyr in proximity to helices $\alpha 3$ (residues 164–159) and $\alpha 3/\beta 3$ loop (residues 157–163) abolishing its inhibitory effect on Aro4. By contrast, Aro3^{K222L} alone doesn't mobilize Phe in the pocket and thus Phe remains inhibitory.

Although the D154 of Aro3 and its counterparts of other type Ia DHAPS are located outside the inhibitor binding cavity^{14,20,28}, substitution by Asn weakened interactions between Q159/K222 and the enzyme inhibitor (Fig. 4). Type Ia DAHPS enzymes share highly similar overall folding and domain architectures, and the D154 of Aro3 was highly conserved in type Ia DAHPS enzymes through multiple sequence alignment (MSA) using the ConSurf Server (https://consurf.tau.ac.il/consurf_index.php). The modeled complex structure and MD simulation taken together suggest that the D to N mutation may endow all type Ia DHAPS enzymes with advantages for evading feedback inhibition in fermenting industry for aromatic compounds. This was supported by our preliminary experiments using the yeast plate assay. The origins of tested DHAPS include *Yarrowia lipolytica*, *Pichia pastoris*, *Kluyveromyces marxianus*, and *Hansenula polymorpha*, each having uniquely attractive properties, high acetyl-CoA contents, high protein production, thermotolerance, and competency in protein glycosylation respectively^{21–24}. Therefore, these microbial organisms started being used as cell factories for various chemical compounds including aromatic products. High levels of resveratrol, scutellarin, and L-tyrosine derivatives have recently been produced by engineered *Yarrowia lipolytica*^{29,30} and *Pichia pastoris* strains³¹. In most of these studies, Aro4^{K229L} from *S. cerevisiae* was introduced into the non-conventional hosts to facilitate carbon fluxes towards AAAs synthetic pathway^{23,29–32}. Our yeast

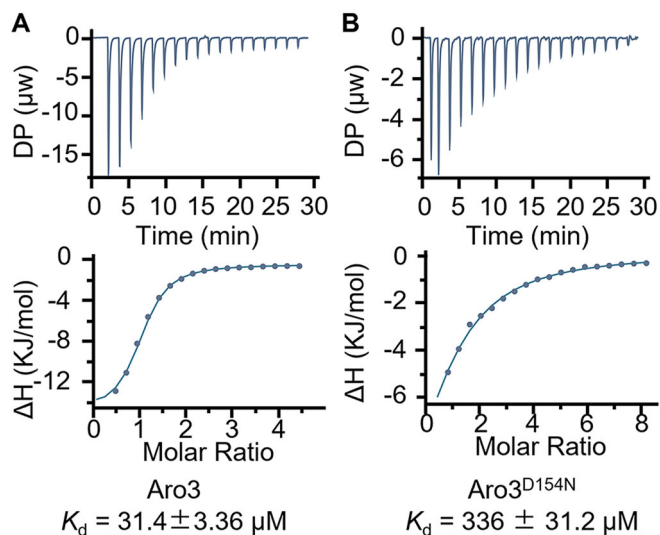


Fig. 5 ITC analysis of L-Phe binding to Aro3 variants. **A, B** ITC titrations of L-Phe to the wild type of Aro3 (**A**) and Aro3^{D154N} (**B**). The upper panels present the binding isotherm and the lower panels show the integrated heat for per mole of injectant as a function of molar ratio.

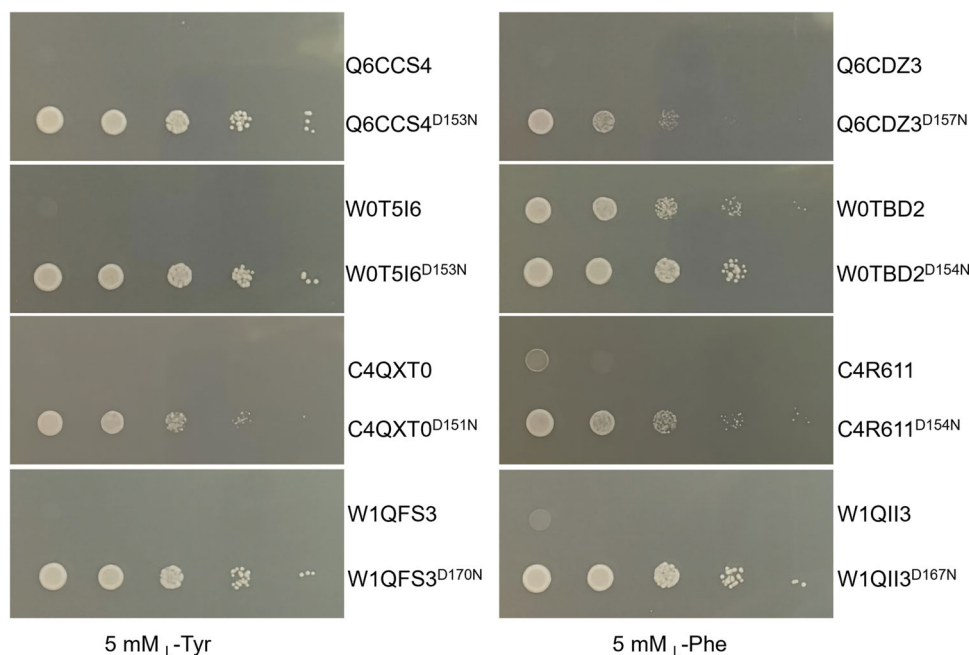


Fig. 6 Growth inhibition by L-Phe or L-Tyr of yeast strains carrying various Type Ia DAHPS enzymes from non-conventional industrial hosts. The restoration of *TRP1* gene and the exchange of the *ARO3* promoter with the constitutive *TEF1* promoter were performed in CEN.PK2-1C Δ aro4 strain, then the genes encoding various Type Ia DAHPS enzymes were integrated into the *ARO3* locus. Q6CCS4 and Q6CDZ3 were encoded by *YIARO4* and *YIARO3* from *Yarrowia lipolytica*; C4QXT0 and C4R611 were encoded by *KpARO4* and *KpARO3* from *Komagataella phaffii* GS115 (*Pichia pastoris*); W0T516 and W0TBD2 were encoded by *KmARO4* and *KmARO3* from *Kluyveromyces marxianus* strain DMKU3-1042 (*Candida kefyr*); W1QFS3 and W1QI13 were encoded by *OpARO4* and *OpARO3* from *Ogataea parapolymorpha* strain ATCC 26012 (*Hansenula polymorpha*), respectively. Mutants of these Type Ia DAHPS enzymes were designed with the analogous D154N of Aro3. The yeast strains were cultivated in MV liquid medium, harvested at 36 h, diluted at OD₆₀₀ = 1.0, and serially 10-fold diluted to spot onto the MV solid medium in the presence of 5 mM L-Phe or L-Tyr. Plates were incubated at 30 °C for 60 h.

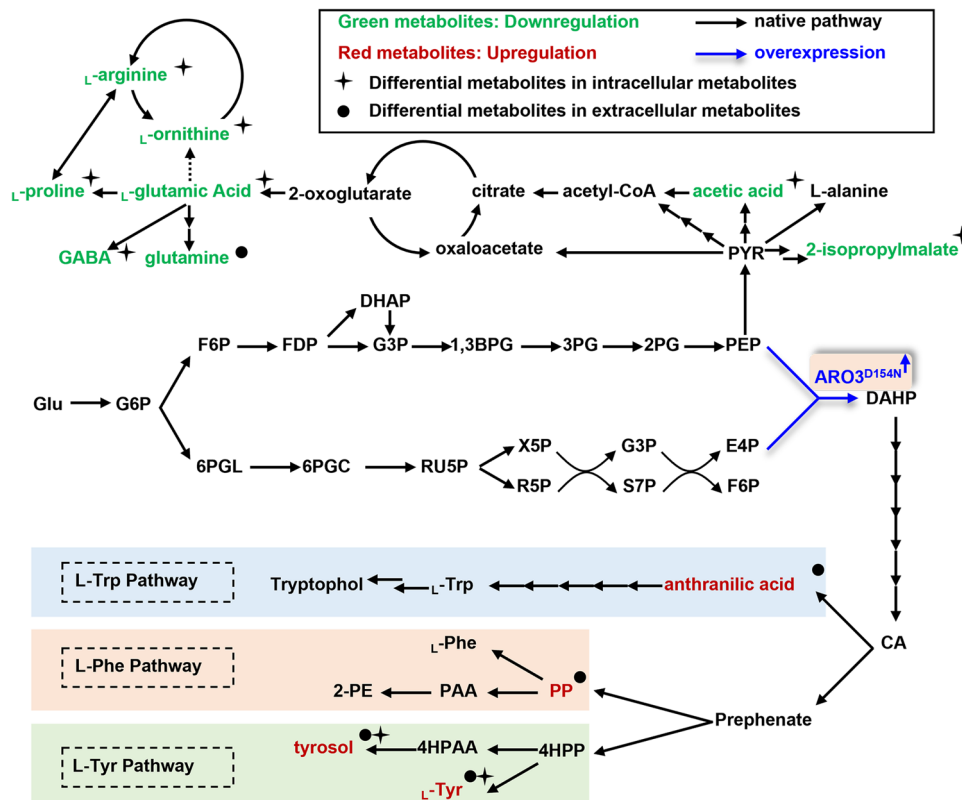


Fig. 7 Differential metabolites between the wild-type strain and the $ARO3^{D154N}$ overexpressing yeast strain. Orthogonal partial least squares discriminant analysis (OPLS-DA) was applied to figure out the differential metabolites between the groups. The downregulated metabolites were colored in green; the upregulated metabolites were in red and the metabolites with insignificant changes were in black. The intracellular and extracellular metabolites with significant differences in overexpressing $ARO3^{D154N}$ yeast strains in comparison to the wild-type strains were marked with asterisk and dot, respectively. Black arrows represent the native pathways in *S. cerevisiae*; blue bold arrow represents the overexpressed gene in this study. Metabolite abbreviations: Glu, glucose; G6P, glucose 6-phosphate; F6P, fructose 6-phosphate; FDP, fructose 1,6-bisphosphate; G3P, D-glyceraldehyde 3-phosphate; DHAP, dihydroxyacetone phosphate; 1,3BPG, 1,3-bisphospho-D-glycerate; 3PG, 3-phospho-D-glycerate; 2PG, 2-phospho-D-glycerate; 6PGL, D-glucono-1,5-lactone 6-phosphate; 6PGC, 6-phospho-D-gluconate; RU5P, D-ribulose 5-phosphate; X5P, D-xylulose 5-phosphate; R5P, D-ribose 5-phosphate; PRPP, 5-phospho-alpha-D-ribose 1-diphosphate; S7P, sedoheptulose 7-phosphate; PEP, phosphoenolpyruvate; E4P, D-Erythrose 4-phosphate; DAHP, 3-deoxy-D-arabino-heptulosonate-7-phosphate; CA, chorismate; PP, phenylpyruvic acid; PAA, phenylacetaldehyde; 2-PE, 2-phenylethanol; L-Phe, L-phenylalanine; 4HPP, 4-hydroxyphenylpyruvic acid; 4HPAA, 4-hydroxyphenylacetaldehyde; L-Tyr, L-tyrosine; L-Trp, L-tryptophan; PYR, pyruvate; GABA, γ -aminobutyric acid.

plate assays were initial attempts to understand the DHAPS from these organisms, which may shed light on further increase of aromatic compound production in non-conventional platforms using their native enzymes. The potential of this feedback-unlocked strategy in industrial hosts was fully displayed by the record-high titers of tyrosol and salidroside in *S. cerevisiae* strains overexpressing $ARO3^{D154N}$.

Methods

Protein expression and purification. The mutants of $ARO3$ were constructed by one-step site-directed mutagenesis method³³ and cloned to pET21 via Gibson cloning³⁴, containing a His₆ tag at the C-terminus. All proteins in this study were expressed in *E. coli* strain Rosetta 2 (DE3). The *E. coli* cells were cultured at 37 °C in LB medium (containing 100 mg/L ampicillin) until OD₆₀₀ reached 0.8, and then induced by 0.2 mM isopropyl β -D-thiogalactopyranoside (IPTG) at 16 °C for 18–20 h. Cells were harvested by centrifugation at 4000 \times g for 12 min, re-suspended in the lysis buffer (20 mM Tris-HCl buffer, pH 8.0, 150 mM NaCl, 10% glycerol), and lysed using a high-pressure French press (Antos Nano Technology Co., Ltd., China). After centrifugation, the supernatant was loaded onto a Nickel-charged nitrilotriacetic acid (NTA) column and the column was washed with the wash buffer (20 mM Tris-HCl buffer, pH 8.0, 150 mM NaCl, 10% glycerol, 10 mM imidazole), and then eluted with the elution buffer (20 mM Tris-HCl buffer, pH 8.0, 150 mM NaCl, 10% glycerol, 250 mM imidazole). The proteins were further purified by gel filtration chromatography (Superdex 200 Increase 10/300 GL, GE Healthcare) with the storage buffer (50 mM potassium phosphate buffer, pH 6.5, 150 mM NaCl). The purified proteins were stored at -80 °C after flash-frozen in liquid nitrogen until use.

Crystallization and structure determination. Crystals were grown using the sitting drop vapor diffusion method at 18 °C by mixing equal volumes (1.5 μ L + 1.5 μ L) of protein solution (8 mg/mL) and crystallization buffer (0.1 M BICINE, pH 9.0, 0.1 M sodium chloride, 20% v/v polyethylene glycol monomethyl ether 550). The data sets were collected at beamline BL19U1 of Shanghai Synchrotron Radiation Facility (SSRF) and processed with the XDS using Aimless to scale in the CCP4 suite. The structure was solved by molecular replacement using the CCP4 suite with the structure model that was predicted by AlphaFold2³⁵ as a template. The final model was refined through multiple cycles of building and refinement and the R_{work}/R_{free} values were 25.2%/29.5%, respectively (Table 1). The protein crystal data is provided with Supplementary Data 1.

Modeling and molecular dynamics simulations. The structural model of Aro3 with L-Phe complex was constructed using AutoDockTools-1.5.6 program. The box was set relative to the binding pocket in the known DAHPS structure complexed with L-Phe (PDB: 1KFL and 4UC5), using the following parameters: grid box center, x, y, z = $-14.959, -35.752, 13.189$; grid box size in x, y, z direction = 20, 20, 30). Other parameters were used as default. Additionally, the selection of the binding mode for further analysis was also based on referencing the known structures (PDB: 1KFL and 4UC5). The molecular dynamics simulations (MD) were built by CHARMM-GUI and run through using Gromacs with the CHARMM36 force field (<http://www.gromacs.org/>)³⁶. The protein was placed into TIP3P water and 0.15 M NaCl (in addition to the counterions used to neutralize charge), and the box size was $117 \times 117 \times 117$ Å³ with periodic boundary conditions. The system was energy minimized using the steepest descents method over 5000 steps. Next, the system was relaxed by applying restraints using the standard CHARMM-GUI equilibration protocol. The simulation was performed for 1000 ns without positional restraints with 2 fs time steps at temperature of 303 K and

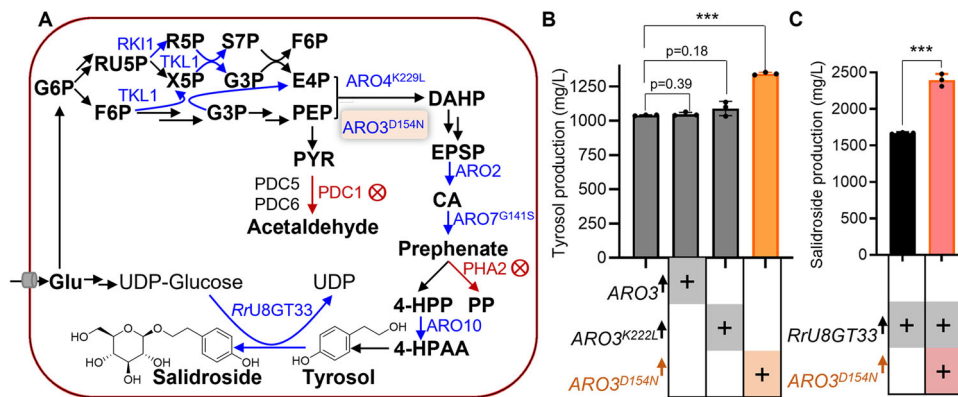


Fig. 8 The overexpression of ARO3^{D154N} enhanced tyrosol and salidroside production in yeast strains. **A** The biosynthetic pathway of tyrosol and salidroside in *S. cerevisiae*. The pentose phosphate pathway, glycolysis, shikimate pathway, and L-tyrosine branch were systematically engineered to relieve the bottlenecks for synthesis of tyrosol^{11, 27}. Blue and red arrows represent the gene overexpression and gene deletion, respectively. The overexpression of ARO3^{D154N} was used to divert carbon flux towards the formation of tyrosol and salidroside. Metabolite abbreviations: Glu, glucose; G6P, glucose-6-phosphate; RU5P, D-ribulose 5-phosphate; X5P, D-xylulose 5-phosphate; R5P, D-ribose 5-phosphate; S7P, sedoheptulose 7-phosphate; G3P, D-glyceraldehyde 3-phosphate; F6P, beta-D-Fructose 6-phosphate; PEP, phosphoenolpyruvate; E4P, D-erythrose 4-phosphate; PYR, pyruvate; DAHP: 3-deoxy-D-arabino-heptulosonate-7-phosphate; EPSP: 5-enolpyruvyl-3-shikimate; CA, chorismate; 4-HPP: 4-hydroxyphenylpyruvate; PP: phenylpyruvate; 4-HPPA: 4-hydroxyphenylacetylaldehyde. **B** The overexpression of ARO3^{D154N} enhanced the tyrosol production. **C** The overexpression of ARO3^{D154N} enhanced the salidroside production. Error bars represent the standard deviation of three biological replicates. Source data are available in Supplementary Data 4. Statistical analysis was performed by using Student's t test (***) $p < 0.001$.

constant pressure (1 bar). The structural coordinates of the initial and final conformation obtained from our simulations are provided with Supplementary Data 2. During the MD process, the LINC algorithm was used to constrain the bond length³⁷. The smoothed cutoff distance for non-bonded interactions was set to 12 Å and long-range electrostatic interactions were computed with the Particle Mesh Ewald (PME) method³⁸.

Isothermal titration calorimetry. For isothermal titration calorimetry (ITC measurement), L-Phe was dissolved in the storage buffer (50 mM potassium phosphate buffer, pH 6.5, 150 mM NaCl). Isothermal titration calorimetry was carried out at 25 °C on an ITC200 system (MicroCal, UK). 8 mM L-Phe was titrated into 200 μM Aro3 protein in storage buffer. A titration of L-Phe into storage buffer was carried out as a control. Data were fitted and analyzed using MicroCal PEAQ-ITC Analysis Software (Malvern Panalytical, UK).

Enzyme assays. The reaction mixture (250 μL) contained 100 mM potassium phosphate buffer (pH 6.5), 0.5 mM phosphoenolpyruvate (PEP) and 0.5 mM erythrose-4-phosphate (E4P). To check the allosteric control of Aro3 variants, either 0.1 mM, 0.5 mM, 1 mM, 2.5 mM, 5 mM, or 10 mM of L-Phe (final concentration) was added to the reaction mixture. The reaction was initiated by the addition of Aro3 protein (2 μg) and was incubated at 30 °C for 5 min. Then the DAHP was detected via the method described by Sprinson³⁹ with some modifications. Firstly, 100 μL of 10% w/v trichloroacetic acid solution was added into the mixture to stop the reaction. Next, the supernatant was obtained by centrifugation at 12,000 × g for 5 min and 125 μL periodic acid (25 mM in 0.125 M H₂SO₄) was added to the supernatant and the mixture was incubated at 25 °C for 45 min. To eliminate excess periodate, 250 μL of 2% (w/v) sodium arsenite in 0.5 M HCl was added into the mixture. After incubation at room temperature for 2 min, 1 mL of 0.3% (w/v) 2-thiobarbituric acid (pH 2.0) was added to the tube and then the tube was heated at 100 °C for 5 min. The pink color developed was rapidly measured at 549 nm by using SynergyMx Multi-Mode Microplate Reader (BioTek, USA).

Strain construction. *S. cerevisiae* strains are listed in Supplementary Table 1. The plasmids used in this study were listed in Supplementary Table 2 and the primers were listed in Supplementary Table 3. The endogenous genes, promoters and terminators of *S. cerevisiae* were amplified from genomic DNA of CEN.PK2-1C. The DNA sequences of AroF, YIARO4/YIARO3, and KpARO4/KpARO3 were cloned from the genomic DNA of *E. coli*, *Yarrowia lipolytica*, and *Komagataella phaffii* GS115, respectively. The genes of KmARO4/KmARO3 and OpARO4/OpARO3 were synthesized by GENEWIZ, China. All the DAHPs sequences were listed at Supplementary Data 3.

Plasmids pTY1-3 were constructed in our previous study¹¹. To construct plasmids pTY4, the plasmid pRS405 was firstly linearized using restriction enzymes HindIII-HF and BamHI-HF (New England Biolabs, US). Then the TEF1 promoter, ARO3 fragment and PGK1 terminator were ligated together through overlap extension PCR and ligated to the linearized pRS405. Plasmids pTY5 and pTY6 harboring ARO3^{K222L} and ARO3^{D154N} respectively were constructed through the

similar procedure. Plasmids pTY4-6 were linearized at their auxotrophic LEU2 marker and integrated at the LEU2 site of yeast. Yeast transformation was carried out through the LiAc/ssDNA/PEG method⁴⁰. The corrected yeast clones were selected on SC-LEU medium. The CRISPR-Cas9 system was applied to modify the genome, which was similar in our previous process¹¹.

Culture conditions. Yeast strains were grown on YPD medium (20 g/L peptone, 10 g/L yeast extract and 20 g/L glucose). The yeast transformants were screened on YPD containing 200 μg/mL G418 or synthetic complete drop-out medium. DH5α and DH10β were used for sub-cloning and Rosetta2 (DE3) was used for protein expression. The *E. coli* strains were cultivated in LB medium with 100 μg/mL ampicillin or 50 μg/mL kanamycin at 37 °C. The MV medium (0.15% yeast nitrogen base, 0.52% ammonium sulfate, 2% glucose, 1% succinic acid, 0.3% KOH (pH 4.0 for liquid medium) or 8.5% KOH (pH = 5.5 for solid medium) was supplemented with histidine, leucine, and uracil to test the feedback sensitivity of L-Phe on Aro3 variants. Yeast strains were cultured in MV liquid medium 36 h, diluted at OD₆₀₀ = 1.0, and then were serially 10-fold diluted to spot onto the MV solid medium in the presence of different concentrations of L-Phe, L-Trp, or L-Tyr. Plates were incubated at 30 °C for 60 h.

Metabolomics analysis. Intracellular and extracellular metabolites were analyzed by Metware Biotech Co., Ltd (Wuhan, China). In brief, yeasts were grown on YPD medium at 30 °C for 48 h, and the cultivated yeasts were centrifuged at 5000 rpm for 5 min. The harvested cells and the supernatant were sent to Metware Biotech Co., Ltd (Wuhan, China) for further analysis. The harvested cells were washed with Milli-Q water and extracted for intracellular metabolites. The supernatant was used for extracellular metabolites analysis. The metabolites were extracted by adding three times of ice-cold methanol and qualitatively analyzed using a LC-MS/MS system. The analytical conditions were as follows, UPLC column, Waters ACQUITY UPLC HSS T3 C18 (1.8 μm, 2.1 mm × 100 mm); column temperature, 40 °C; flow rate, 0.4 mL/min; injection volume, 2 μL; solvent system, water (0.1% formic acid): acetonitrile (0.1% formic acid); gradient program, 95:5 V/V at 0 min, 10:90 V/V at 11.0 min, 10:90 V/V at 12.0 min, 95:5 V/V at 12.1 min, 95:5 V/V at 14.0 min. Each biological sample was measured in triplicates.

Fermentation and analysis of products. Yeast strains were picked from pre-cultured plates and cultured in 4 mL YPD medium at 30 °C, shaking at 220 rpm for 24 h. Portions of pre-cultured mixture were then transferred into 50 mL YPD medium in 250 mL shake flasks until the OD₆₀₀ reached ~0.2. The strains were cultured at 30 °C, shaking at 220 rpm for 84 h. 1 mL of the culture was collected and centrifuged at 5000 rpm for 5 min. The supernatant was stored at -20 °C until analysis.

Tyrosol, salidroside, tryptophol, and 2-phenylethanol were analyzed using an Agilent HPLC 1260 series instrument equipped with a Zorbax SB-C18 column (Agilent, 5 μm, 4.6 mm × 250 mm). The injection volume was 10 μL, and samples were maintained at 30 °C. A diode array detector (DAD) was used for the analysis (identification and quantification) of the compounds. Mobile phase A was 0.05% formic acid in water and solvent B was acetonitrile, and phase A and phase B were

used for following analysis. The flow rate was set to 1.0 mL/min. Tyrosol and salidroside were analyzed by using a gradient method with two solvents: 8% B for 18 min, 5% B for 2 min, 5–95% B in 10 min, 95% B for 5 min, and 8% B for 5 min. The absorbance was set at 224 nm. For the analysis of 2-phenylethanol, the profile was as follows: 40% B for 20 min, 5% B for 5 min, 5–95% B in 5 min, and finally return to 40% B for 10 min. The absorbance of 2-phenylethanol was set at 210 nm. For the analysis of tryptophol, samples were analyzed for 50 min using the following gradient method: 8% B for 18 min, 25% B for 16 min, 95% B for 4 min, and 8% B for 10 min. The absorbance of tryptophol was set at 210 nm. The products were analyzed using an LC-ESI-MS/MS system (Nexera UHPLC LC-30A and AB SCIEX Triple Quad 5500 system). The Hypersil GOLD C18 column (1.9 μ m, 100 mm \times 2.1 mm; Thermo Fisher Scientific, USA) were used to separate tyrosol and salidroside in samples. The samples were maintained at 35 °C. The flow rate was 0.4 mL/min, and the injection volume was 1.0 μ L. The mobile phases were 0.1% formic acid in water (A) and acetonitrile (B). The mobile phase for the products analysis was 2% B, which was applied for 5.0 min. For the MS2 model, the daughter ion of tyrosol (m/z , 137.1) and salidroside (m/z , 299.1) was scanned for in the range 50–200, 50–350, respectively.

Reporting summary. Further information on research design is available in the Nature Portfolio Reporting Summary linked to this article.

Data availability

The atomic coordinates and structure factors have been deposited in the Protein Data Bank (<https://www.rcsb.org/>) with PDB ID code 7YKC. The protein crystal data were also provided with Supplementary Data 1. The structural coordinates of the initial conformation and every 100 ns conformation obtained from our simulations are provided with Supplementary Data 2. Gene sequences were listed at Supplementary Data 3. Source data are available in Supplementary Data 4.

Received: 8 March 2023; Accepted: 30 June 2023;

Published online: 15 July 2023

References

- Cao, M., Gao, M., Suastegui, M., Mei, Y. & Shao, Z. Building microbial factories for the production of aromatic amino acid pathway derivatives: from commodity chemicals to plant-sourced natural products. *Metab. Eng.* **58**, 94–132 (2020).
- Srinivasan, P. & Smolke, C. D. Biosynthesis of medicinal tropane alkaloids in yeast. *Nature* **585**, 614–619 (2020).
- Yokoyama, R., Kleven, B., Gupta, A., Wang, Y. & Maeda, H. A. 3-Deoxy-D-arabino-heptulosonate 7-phosphate synthase as the gatekeeper of plant aromatic natural product biosynthesis. *Curr. Opin. Plant Biol.* **67**, 102219 (2022).
- Sun, J., Sun, W., Zhang, G., Lv, B. & Li, C. High efficient production of plant flavonoids by microbial cell factories: challenges and opportunities. *Metab. Eng.* **70**, 143–154 (2022).
- Jiao, W., Lang, E. J., Bai, Y., Fan, Y. & Parker, E. J. Diverse allosteric componentry and mechanisms control entry into aromatic metabolite biosynthesis. *Curr. Opin. Struct. Biol.* **65**, 159–167 (2020).
- Hartmann, M. et al. Evolution of feedback-inhibited beta/alpha barrel isoenzymes by gene duplication and a single mutation. *Proc. Natl Acad. Sci. USA* **100**, 862–867 (2003).
- Luttik, M. A. et al. Alleviation of feedback inhibition in *Saccharomyces cerevisiae* aromatic amino acid biosynthesis: quantification of metabolic impact. *Metab. Eng.* **10**, 141–153 (2008).
- Kikuchi, Y., Tsujimoto, K. & Kurahashi, O. Mutational analysis of the feedback sites of phenylalanine-sensitive 3-deoxy-D-arabino-heptulosonate-7-phosphate synthase of *Escherichia coli*. *Appl Environ. Microbiol.* **63**, 761–762 (1997).
- Yang, J. et al. Harnessing the endogenous 2 μ plasmid of *Saccharomyces cerevisiae* for pathway construction. *Front. Microbiol.* **12**, 679665 (2021).
- Bruckner, C., Oreb, M., Kunze, G., Boles, E. & Tripp, J. An expanded enzyme toolbox for production of cis, cis-muconic acid and other shikimate pathway derivatives in *Saccharomyces cerevisiae*. *FEMS Yeast Res.* **18**, <https://doi.org/10.1093/femsyr/foy017> (2018).
- Liu, H. et al. Multi-modular engineering of *Saccharomyces cerevisiae* for high-titre production of tyrosol and salidroside. *Micro. Biotechnol.* **14**, 2605–2616 (2021).
- Hassing, E. J., de Groot, P. A., Marquenie, V. R., Pronk, J. T. & Daran, J. G. Connecting central carbon and aromatic amino acid metabolisms to improve de novo 2-phenylethanol production in *Saccharomyces cerevisiae*. *Metab. Eng.* **56**, 165–180 (2019).
- Xiao, F. et al. Metabolic engineering of *Saccharomyces cerevisiae* for high-level production of chlorogenic acid from glucose. *ACS Synth. Biol.* **11**, 800–811 (2022).
- Shumilin, I. A., Zhao, C., Bauerle, R. & Kretsinger, R. H. Allosteric inhibition of 3-deoxy-D-arabino-heptulosonate-7-phosphate synthase alters the coordination of both substrates. *J. Mol. Biol.* **320**, 1147–1156 (2002).
- Kunzler, M., Springer, C. & Braus, G. H. Activation and repression of the yeast ARO3 gene by global transcription factors. *Mol. Microbiol.* **15**, 167–178 (1995).
- Shumilin, I. A., Kretsinger, R. H. & Bauerle, R. H. Crystal structure of phenylalanine-regulated 3-deoxy-D-arabino-heptulosonate-7-phosphate synthase from *Escherichia coli*. *Structure* **7**, 865–875 (1999).
- Wagner, T., Shumilin, I. A., Bauerle, R. & Kretsinger, R. H. Structure of 3-deoxy-D-arabino-heptulosonate-7-phosphate synthase from *Escherichia coli*: comparison of the Mn⁽²⁺⁾*2-phosphoglycolate and the Pb⁽²⁺⁾*2-phosphoenolpyruvate complexes and implications for catalysis. *J. Mol. Biol.* **301**, 389–399 (2000).
- Konig, V., Pfeil, A., Braus, G. H. & Schneider, T. R. Substrate and metal complexes of 3-deoxy-D-arabino-heptulosonate-7-phosphate synthase from *Saccharomyces cerevisiae* provide new insights into the catalytic mechanism. *J. Mol. Biol.* **337**, 675–690 (2004).
- Cross, P. J. et al. *Neisseria meningitidis* expresses a single 3-deoxy-D-arabino-heptulosonate 7-phosphate synthase that is inhibited primarily by phenylalanine. *Protein Sci.* **22**, 1087–1099 (2013).
- Cui, D. et al. Molecular basis for feedback inhibition of tyrosine-regulated 3-deoxy-D-arabino-heptulosonate-7-phosphate synthase from *Escherichia coli*. *J. Struct. Biol.* **206**, 322–334 (2019).
- Sun, L. & Alper, H. S. Non-conventional hosts for the production of fuels and chemicals. *Curr. Opin. Chem. Biol.* **59**, 15–22 (2020).
- Patra, P., Das, M., Kundu, P. & Ghosh, A. Recent advances in systems and synthetic biology approaches for developing novel cell-factories in non-conventional yeasts. *Biotechnol. Adv.* **47**, 107695 (2021).
- Larroude, M., Nicaud, J. M. & Rossignol, T. *Yarrowia lipolytica* chassis strains engineered to produce aromatic amino acids via the shikimate pathway. *Micro. Biotechnol.* **14**, 2420–2434 (2021).
- Cai, P. et al. Methanol biotransformation toward high-level production of fatty acid derivatives by engineering the industrial yeast *Pichia pastoris*. *Proc. Natl Acad. Sci. USA* **119**, e2201711119 (2022).
- Karkovic Markovic, A., Toric, J., Barbaric, M. & Jakobusic Brala, C. Hydroxytyrosol, tyrosol and derivatives and their potential effects on human health. *Molecules* **24**, <https://doi.org/10.3390/molecules24102001> (2019).
- Zhang, X. et al. Salidroside: a review of its recent advances in synthetic pathways and pharmacological properties. *Chem. Biol. Interact.* **339**, 109268 (2021).
- Liu, H. et al. High-level production of hydroxytyrosol in engineered *Saccharomyces cerevisiae*. *ACS Synth. Biol.* **11**, 3706–3713 (2022).
- Lang, E. J., Heyes, L. C., Jameson, G. B. & Parker, E. J. Calculated pK_a variations expose dynamic allosteric communication networks. *J. Am. Chem. Soc.* **138**, 2036–2045 (2016).
- Saez-Saez, J. et al. Engineering the oleaginous yeast *Yarrowia lipolytica* for high-level resveratrol production. *Metab. Eng.* **62**, 51–61 (2020).
- Wang, Y. et al. Metabolic engineering of *Yarrowia lipolytica* for scutellarin production. *Synth. Syst. Biotechnol.* **7**, 958–964 (2022).
- Kumokita, R. et al. Construction of an L-tyrosine chassis in *Pichia pastoris* enhances aromatic secondary metabolite production from glycerol. *ACS Synth. Biol.* **11**, 2098–2107 (2022).
- Gao, M. et al. Innovating a nonconventional yeast platform for producing shikimate as the building block of high-value aromatics. *ACS Synth. Biol.* **6**, 29–38 (2017).
- Zheng, L., Baumann, U. & Reymond, J. L. An efficient one-step site-directed and site-saturation mutagenesis protocol. *Nucleic Acids Res.* **32**, e115 (2004).
- Gibson, D. G. et al. Enzymatic assembly of DNA molecules up to several hundred kilobases. *Nat. Methods* **6**, 343–345 (2009).
- Jumper, J. et al. Highly accurate protein structure prediction with AlphaFold. *Nature* **596**, 583–589 (2021).
- Huang, J. & MacKerell, A. D. Jr CHARMM36 all-atom additive protein force field: validation based on comparison to NMR data. *J. Comput. Chem.* **34**, 2135–2145 (2013).
- Hess, B. P-LINCS: a parallel linear constraint solver for molecular simulation. *J. Chem. Theory Comput.* **4**, 116–122 (2008).
- Harvey, M. J. & De Fabritiis, G. An implementation of the smooth particle Mesh Ewald Method on GPU hardware. *J. Chem. Theory Comput.* **5**, 2371–2377 (2009).
- Sprinson, D. B., Srinivasan, P. & Katagiri, M. In *Methods in Enzymology* Vol. 5, 394–398 (Elsevier, 1962).
- Gietz, R. D. & Schiestl, R. H. High-efficiency yeast transformation using the LiAc/SS carrier DNA/PEG method. *Nat. Protoc.* **2**, 31–34 (2007).

Acknowledgements

The work was supported by the National Key Research and Development Program of China (Grant No. 2018YFA0903300), the National Natural Science Foundation of China

(Grant No. 32071426), and the Key-Area Research and Development Program of Guangdong Province (2020B0303070002).

Author contributions

H.L. and Y.L. designed the experiments. H.L. performed the strain construction, fermentation, protein purification, crystallization, and ITC assays; Q.X. performed the molecular dynamics simulations; X.W., H.M., J.L., X.G., and Z.L. contributed to the in vivo and in vitro assays. H.L., Y.Z., and Y.L. wrote the manuscript.

Competing interests

Y.L. and H.L. have lodged an application for a patent on the use of the Aro3 mutant reported in this study (CN113174375B, China). All other authors declare no competing interests.

Additional information

Supplementary information The online version contains supplementary material available at <https://doi.org/10.1038/s42004-023-00946-x>.

Correspondence and requests for materials should be addressed to Yunzi Luo.

Peer review information *Communications Chemistry* thanks Robert Phillips and the other, anonymous, reviewers for their contribution to the peer review of this work.

Reprints and permission information is available at <http://www.nature.com/reprints>

Publisher's note Springer Nature remains neutral with regard to jurisdictional claims in published maps and institutional affiliations.



Open Access This article is licensed under a Creative Commons Attribution 4.0 International License, which permits use, sharing, adaptation, distribution and reproduction in any medium or format, as long as you give appropriate credit to the original author(s) and the source, provide a link to the Creative Commons licence, and indicate if changes were made. The images or other third party material in this article are included in the article's Creative Commons licence, unless indicated otherwise in a credit line to the material. If material is not included in the article's Creative Commons licence and your intended use is not permitted by statutory regulation or exceeds the permitted use, you will need to obtain permission directly from the copyright holder. To view a copy of this licence, visit <http://creativecommons.org/licenses/by/4.0/>.

© The Author(s) 2023